

The Cosmic Microwave Background Anisotropy Power Spectrum measured by Archeops

A. Benoît¹, P. Ade², A. Amblard^{3,24}, R. Ansari⁴, É. Aubourg^{5,24}, S. Bargout⁴, J. G. Bartlett^{3,24}, J.-Ph. Bernard^{6,7}, R. S. Bhatia⁸, A. Blanchard⁶, J. J. Bock^{8,9}, A. Boscaleri¹⁰, F. R. Bouchet¹¹, A. Bourrachot⁴, P. Camus¹, F. Couchot⁴, P. de Bernardis¹², J. Delabrouille^{3,24}, F.-X. Désert¹³, O. Doré¹¹, M. Douspis^{6,14}, L. Dumoulin¹⁵, X. Dupac¹⁶, P. Filliatre¹⁷, P. Fosalba¹¹, K. Ganga¹⁸, F. Gannaway², B. Gautier¹, M. Giard¹⁶, Y. Giraud-Héraud^{3,24}, R. Gispert^{7†*}, L. Guglielmi^{3,24}, J.-Ch. Hamilton^{3,17}, S. Hanany¹⁹, S. Henrot-Versillé⁴, J. Kaplan^{3,24}, G. Lagache⁷, J.-M. Lamarre⁷, A. E. Lange⁸, J. F. Macías-Pérez¹⁷, K. Madet¹, B. Maffei², Ch. Magneville^{5,24}, D. P. Marrone¹⁹, S. Masi¹², F. Mayet⁵, A. Murphy²⁰, F. Naraghi¹⁷, F. Nati¹², G. Patanchon^{3,24}, G. Perrin¹⁷, M. Piat⁷, N. Ponthieu¹⁷, S. Prunet¹¹, J.-L. Puget⁷, C. Renault¹⁷, C. Rosset^{3,24}, D. Santos¹⁷, A. Starobinsky²¹, I. Strukov²², R. V. Sudiwala², R. Teyssier^{11,23}, M. Tristram¹⁷, C. Tucker², J.-C. Vanel^{3,24}, D. Vibert¹¹, E. Wakui², and D. Yvon^{5,24}

¹ Centre de Recherche sur les Très Basses Températures, BP166, 38042 Grenoble Cedex 9, France

² Cardiff University, Physics Department, PO Box 913, 5, The Parade, Cardiff, CF24 3YB, UK

³ Physique Corpusculaire et Cosmologie, Collège de France, 11 pl. M. Berthelot, F-75231 Paris Cedex 5, France

⁴ Laboratoire de l'Accélérateur Linéaire, BP 34, Campus Orsay, 91898 Orsay Cedex, France

⁵ CEA-CE Saclay, DAPNIA, Service de Physique des Particules, Bat 141, F-91191 Gif sur Yvette Cedex, France

⁶ Laboratoire d'Astrophysique de l'Obs. Midi-Pyrénées, 14 Avenue E. Belin, 31400 Toulouse, France

⁷ Institut d'Astrophysique Spatiale, Bât. 121, Université Paris XI, 91405 Orsay Cedex, France

⁸ California Institute of Technology, 105-24 Caltech, 1201 East California Blvd, Pasadena CA 91125, USA

⁹ Jet Propulsion Laboratory, 4800 Oak Grove Drive, Pasadena, California 91109, USA

¹⁰ IROE-CNR, Via Panciatichi, 64, 50127 Firenze, Italy

¹¹ Institut d'Astrophysique de Paris, 98bis, Boulevard Arago, 75014 Paris, France

¹² Gruppo di Cosmologia Sperimentale, Dipartimento di Fisica, Università "La Sapienza", P. A. Moro, 2, 00185 Roma, Italy

¹³ Laboratoire d'Astrophysique, Obs. de Grenoble, BP 53, 38041 Grenoble Cedex 9, France

¹⁴ Nuclear and Astrophysics Laboratory, Keble Road, Oxford, OX1 3RH, UK

¹⁵ CSNSM-IN2P3, Bât 108, 91405 Orsay Campus, France

¹⁶ Centre d'Étude Spatiale des Rayonnements, BP 4346, 31028 Toulouse Cedex 4, France

¹⁷ Institut des Sciences Nucléaires, 53 Avenue des Martyrs, 38026 Grenoble Cedex, France

¹⁸ Infrared Processing and Analysis Center, Caltech, 770 South Wilson Avenue, Pasadena, CA 91125, USA

¹⁹ School of Physics and Astronomy, 116 Church St. S.E., University of Minnesota, Minneapolis MN 55455, USA

²⁰ Experimental Physics, National University of Ireland, Maynooth, Ireland

²¹ Landau Institute for Theoretical Physics, 119334 Moscow, Russia

²² Space Research Institute, Profsoyuznaya St. 84/32, Moscow, Russia

²³ CEA-CE Saclay, DAPNIA, Service d'Astrophysique, Bat 709, F-91191 Gif sur Yvette Cedex, France

²⁴ Fédération de Recherche APC, Université Paris 7, Paris, France

February 7, 2020

Abstract. We present a determination by the Archeops experiment of the angular power spectrum of the cosmic microwave background anisotropy in 16 bins over the multipole range $\ell = 15 - 350$. Archeops was conceived as a precursor of the Planck HFI instrument by using the same optical design and the same technology for the detectors and their cooling. Archeops is a balloon-borne instrument consisting of a 1.5 m aperture diameter telescope and an array of 21 photometers maintained at ~ 100 mK that are operating in 4 frequency bands centered at 143, 217, 353 and 545 GHz. The data were taken during the Arctic night of February 7, 2002 after the instrument was launched by CNES from Esrange base (Sweden). The entire data cover $\sim 30\%$ of the sky. This first analysis was obtained with a small subset of the dataset using the most sensitive photometer in each CMB band (143 and 217 GHz) and 12.6% of the sky at galactic latitudes above 30 degrees where the foreground contamination is measured to be negligible. The large sky coverage and medium resolution (better than 15 arcminutes) provide for the first time a high signal-to-noise ratio determination of the power spectrum over angular scales that include both the first acoustic peak and scales probed by COBE/DMR. With a binning of $\Delta\ell=7$ to 25 the error bars are dominated by sample variance for ℓ below 200. A companion paper details the cosmological implications.

Key words. Cosmic microwave background – Cosmology: observations – Submillimeter

1. Introduction

Observations of the Cosmic Microwave Background (CMB) temperature anisotropies have provided answers to fundamental questions in cosmology. The observational determination of the CMB angular power spectrum has already led to important insights on the structure and evolution of the universe. Most notable are the conclusions that the geometry of space is essentially flat (Miller *et al.* 1999, de Bernardis *et al.* 2000, Hanany *et al.* 2000) and that the measurements are consistent with the inflationary paradigm (Netterfield *et al.* 2002, Lee *et al.* 2001, Halverson *et al.* 2002, Sievers *et al.* 2002, Rubiño-Martin *et al.* 2002). Since the first detection of CMB anisotropy with COBE/DMR (Smoot *et al.* 1992), a host of experiments have measured the spectrum down to sub-degree scales, but measurements at large angular scales remain difficult, due to the large sky coverage required to access these modes. This difficulty will be overcome by the future full-sky space missions MAP and Planck.

This paper presents the first results from Archeops, an experiment designed to obtain large sky coverage in a single balloon flight. A detailed description of the instrument inflight performance will be given in Benoît *et al.* (2002c); here we provide only essential information. Archeops¹ is a balloon-borne experiment with a 1.5 m off-axis Gregorian telescope capable of providing a beam of 8' full-width at half-maximum (FWHM) at 143 GHz, and with a bolometric array of 21 photometers operating at frequency bands centered at 143 GHz (8 bolometers), 217 GHz (6), 353 GHz (6=3 polarized pairs) and 545 GHz (1). The focal plane is maintained at a temperature of $\sim 100\text{mK}$ using a ³He-⁴He dilution cryostat. Observations are carried out by turning the payload at 2 rpm in circular scans at a fixed elevation of ~ 41 deg. Observations of a single night cover a large fraction of the sky as the circular scans drift across the sky due to the rotation of the Earth. The instrument was flown successfully three times, from Trapani (Sicily) in July 1999 (Benoît *et al.* 2002a), from Kiruna (Sweden) in January 2001, from Sweden again in February 2002. The analysis here concentrates on the data from the third flight and from only one detector at 217 GHz and one at 143 GHz, which gave the highest CMB sensitivity of 150 and 90 $\mu\text{K}_{\text{CMB}}\cdot\text{s}^{1/2}$ respectively.

2. Observations and processing of the data

The experiment was launched on February 7, 2002 by the CNES² from the Swedish balloon base in ESRANGE, near Kiruna, Sweden, 68°N, 20°E. It reached a float

Send offprint requests to: reprints@archeops.org

* Richard Gispert passed away few weeks after his return from the early mission to Trapani

Correspondence to: benoit@archeops.org

¹ see <http://www.archeops.org>.

² Centre National d'Études Spatiales, the French national space agency

altitude of ~ 34 km and landed 21.5 hours later in Siberia near Noril'sk, where it was recovered by a Franco-Russian team. The night-time scientific observations span 11.7 hours of integration from 15.3 UT to 3.0 UT the next day. Fig. 1 shows the northern galactic part of the sky observed during the flight.

Pointing reconstruction is performed using data from a coaligned optical telescope. About 200 stars are used per revolution to reconstruct the optical telescope attitude and provide a pointing accuracy better than 1 arcminute r.m.s. The pointing alignment offset for each photometer is obtained by observing Jupiter. A fraction of less than 0.1 % of the data corresponding to a bad pointing quality (r.m.s worse than 1.5') were flagged and discarded from the CMB analysis.

The raw Time Ordered Information (TOI), sampled at 153 Hz, are decompressed, then filtered to take into account the AC biasing scheme coming from the readout electronics. Cosmic rays, electronic spikes, artifacts, and noisy data are detected and flagged with an automatic algorithm followed by visual inspection. The flagged data representing less than 1.5% of the data are replaced by a constrained realisation of noise for subsequent detrending and high-pass filtering. The data are corrected with a bolometer model for drifts of the instrument response due to changes in the background optical loading and in the temperature of the focal plane. Low frequency drifts due to airmass and temperature fluctuations of the various stages of the cryostat are decorrelated using housekeeping data (altitude, attitude, temperatures). Furthermore, the CMB dipole, which dominates the signal around $f_{\text{spin}} \simeq 0.03$ Hz for the CMB photometers (143 and 217 GHz), and a spin synchronous atmospheric signal correlated to elevation are subtracted from the data. The data streams are then deconvolved from the photometer time constants as measured on Jupiter and Saturn. To remove residual dust and atmospheric signal in the interval 0.5–2 Hz, the data from the CMB photometers are decorrelated with a linear combination of the high frequency photometers and synthetic dust timeline obtained by observation of a Galactic template³ (Schlegel *et al.* 1998).

The CMB dipole that is detected in the data is the prime calibrator of the instrument. The absolute calibration error against the dipole measured by COBE/DMR (Smoot *et al.* 1992) is less than 4% and less than 8% in temperature at 143 GHz and 217 GHz, respectively. The main uncertainty comes from a parasitic signal in phase with the CMB dipole at f_{spin} . It is estimated using higher frequency non-CMB channels. Two other independent calibration methods, both with intrinsic uncertainty of $\sim 10\%$, give responsivities relative to the dipole calibration at 143 and 217 GHz of -5 and +6% (Jupiter) and -20 and -5% (COBE-FIRAS Galactic Plane

³ The high frequency photometers contain mainly atmospheric signal and Galactic dust which do not have the same frequency behaviour, they therefore have to be decorrelated separately.

Archeops KS3 CMB map

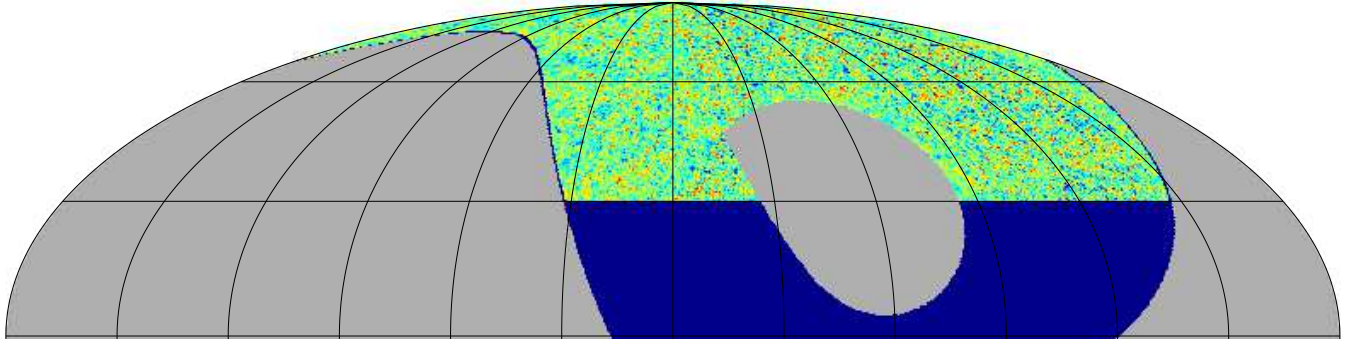


Fig. 1. Archeops CMB map (Galactic coordinates, north hemisphere) in HEALPIX pixelisation (Gorski *et al.* 1998) with 15 arcminutes pixels and a 15 arcminutes Gaussian smoothing. The map was made by coadding the data from 2 photometers as discussed in the text. The dark blue region is not included in the present analysis because of possible contamination by dust. The Galactic anticenter is at the center of the map. The colors in the map range from -500 to 500 μK_{CMB} .

emission), respectively. The beam shapes of the photometers have been measured using in-flight observations of Jupiter. They are moderately elliptical, having a ratio of the major to minor axis of less than 1.2 and 1.5 for the 143 GHz and 217 GHz photometers respectively, and have an equivalent FWHM of 11 and 13 arcminutes, respectively. The error in beam size is less than 10%. An effective symmetrical beam shape is accounted for in the power spectrum analysis. A detailed description of the data processing pipeline will be given in Benoît *et al.* (2002d).

3. Analysis

For the analysis in this paper, only pixels above a Galactic latitude of 30 degrees are considered, giving a total of $\sim 100,000$ 15 arcminutes pixels (HEALPIX $n_{\text{side}}=256$) covering 12.6% of the sky (see Fig. 1). Other regions begin to be contaminated by foreground sources.

Our main method for extracting the CMB power spectrum is an application of the MASTER approach (Hivon *et al.* 2001) that achieves speed by employing sub-optimal map-making and spectral determinations. It is well adapted to the large dataset and permits significant time-domain filtering and a frequentist error estimate of the final power spectrum. The analysis approach assumes that the instrument noise is Gaussian and stationary. We checked this assumption on a subset of data that was selected for CMB analysis. Tests in both time and frequency space include statistical comparison of the data with realistic simulations. A small, slow ($\sim 0.5\%$ /hour) drift of the noise r.m.s. level due to the slow drift of the focal plane temperature was observed and accounted for in the power spectrum estimation.

The measured asymmetric beam for each photometer was taken into account in the analysis by using simulations to determine an effective symmetrical beam transfer function B_ℓ . This transfer function, which was used in the

MASTER CMB simulations, was in excellent agreement with analytical estimates (Fosalba *et al.* 2002).

3.1. Noise power spectrum estimation

First, the Fourier noise power spectrum is estimated for each photometer. Signal contamination is avoided by subtracting the data projected onto a map (and then re-read with the scanning strategy) from the initial TOI. This raw noise power spectrum is then corrected for two important effects (Benoît *et al.* 2002e): (i) pixelisation of the Galactic signal that leads to an overestimate of the noise power spectrum (Doré *et al.* 2001): sub-pixel frequencies of the signal are not subtracted from the initial TOI leaving extra signal at high frequency; (ii) due to the finite number of samples per pixel, noise remains in the map and is subtracted from the initial TOI, inducing an underestimation of the actual noise in the final TOI (Ferreira *et al.* 1999, Stompor *et al.* 2001). Simulations, including realistic noise, Galactic dust and CMB anisotropies, indicate that both corrections are independent of the shape of the true, underlying noise power spectrum, and thus permit an unbiased estimate of the latter with an accuracy better than 1% at all frequencies. The corresponding uncertainty in the noise power spectrum estimation is included in the error bars of the C_ℓ spectrum.

3.2. Map-making

The data are bandpassed between 0.3 and 45 Hz, corresponding to about 30 degrees and 15 arcminutes scales, respectively. The high-pass filter removes remaining atmospheric and galactic contamination, the low-pass filter suppresses non-stationary high frequency noise. The filtering is done in such a way that ringing effects of the signal on bright compact sources (mainly the Galactic plane) are

smaller than $\sim 36 \mu\text{K}^2$ on the CMB power spectrum in the very first ℓ -bin, and negligible for larger multipoles. Filtered TOIs of each absolutely calibrated detector are co-added on the sky to form detector maps. The map shown in Fig. 1 is obtained by combining the maps of each of the photometers. A $1/\sigma^2$ weighting of the data was done in each pixel, where σ^2 is the variance of the data in that pixel. This map shows significant extra variance compared to the difference map on degree angular scales which is attributed to sky-stationary signal.

3.3. CMB power spectrum estimation

Sixteen flat-band powers in bins ranging from $\ell = 15$ to $\ell = 350$ are estimated. The window functions derived from the multipole binning and renormalized to equal amplitude for clarity are shown at the bottom of Fig. 3. They are nearly top-hat functions due to the large sky coverage. The bins can therefore be approximated as independent: off-diagonal terms in the covariance matrix are less than $\sim 12\%$. For the purpose of estimating the power spectrum we made a map that combines the data of the two photometers using two different weighting techniques. Up to $\ell = 310$ the data of each photometer has equal weight and at larger ℓ values the data is noise weighted. This procedure is valid because the multipole bins are nearly independent. The procedure is advantageous because it minimizes the overall statistical noise over the entire ℓ spectrum; equal weighting gives smaller error bars at small ℓ 's and noise weighting gives smaller error bars at large ℓ .

4. Results and robustness tests

The Archeops power spectrum is presented in Fig. 2 and in Tab. 1. Two different binnings corresponding to overlapping, shifted window functions (therefore not independent) were used. Archeops provides the highest ℓ resolution ($\Delta\ell$ from 7 to 25) and most precise measurement of the angular power spectrum for $15 < \ell < 300$ to date. Sample-variance contributes 50% or more of the total statistical error up to $\ell \sim 200$.

The Archeops scanning strategy (large circles on the sky) provides a simple and robust test of systematic errors and data analysis procedures: by changing the sign of the filtered TOIs every other circle, a TOI that should not contain any signal is obtained once it is projected on the sky. This TOI has the same noise power spectrum as the original one. This null test is referred to as the self-difference (SD) test. The angular power spectrum of such a dataset should be consistent with zero at all multipoles because successive circles greatly overlap. This test has been performed with the two photometers independently. The spectra are consistent with zero at all modes: χ^2/ndf of 21/16 and 27/16 for 143 GHz and 217 GHz photometers respectively. Performed on the two-photometers co-added map, the same test gives a power spectrum consistent with zero, with a χ^2/ndf of 25/16 (see Fig. 2). These results show that there is no significant correlated noise among

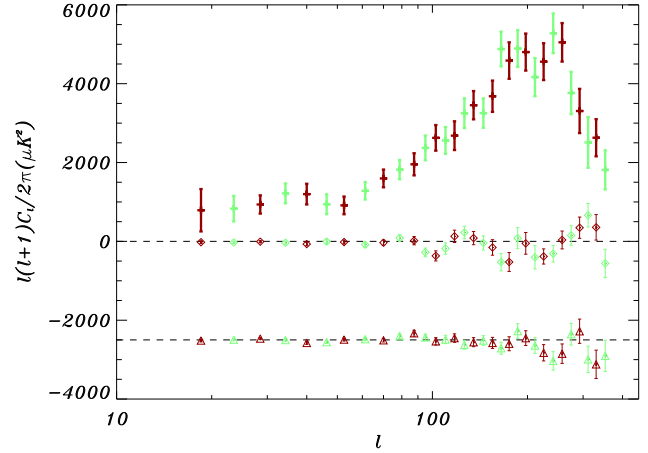


Fig. 2. The Archeops CMB power spectrum for the combination of the two photometers. Green and red data points correspond to two overlapping binnings and are therefore not independent. The light open diamonds show the null test resulting from the self difference (SD) of both photometers and the light open triangles correspond to the difference (D) of both photometers (shifted by $-2500 \mu\text{K}^2$ for clarity) as described in sect. 4 and shown in Tab. 1.

ℓ_{\min}	ℓ_{\max}	$\frac{\ell(\ell+1)C_\ell}{(2\pi)} (\mu\text{K})^2$	SD $(\mu\text{K})^2$	D $(\mu\text{K})^2$
15	22	789 ± 537	-21 ± 34	-14 ± 34
22	35	936 ± 230	-6 ± 25	34 ± 21
35	45	1198 ± 262	-69 ± 45	-75 ± 35
45	60	912 ± 224	-18 ± 50	9 ± 37
60	80	1596 ± 224	-33 ± 63	-8 ± 44
80	95	1954 ± 280	17 ± 105	169 ± 75
95	110	2625 ± 325	-368 ± 128	-35 ± 92
110	125	2681 ± 364	127 ± 156	46 ± 107
125	145	3454 ± 358	82 ± 166	-57 ± 114
145	165	3681 ± 396	-154 ± 196	-75 ± 140
165	185	4586 ± 462	-523 ± 239	-97 ± 177
185	210	4801 ± 469	-50 ± 276	44 ± 187
210	240	4559 ± 467	-382 ± 192	-326 ± 206
240	275	5049 ± 488	35 ± 226	-349 ± 247
275	310	3307 ± 560	346 ± 269	220 ± 306
310	350	2629 ± 471	356 ± 323	-619 ± 358

Table 1. The Archeops CMB power spectrum for the best two photometers (third column). Data points given in this table correspond to the red points in Fig. 2. The fourth column shows the power spectrum for the self difference (SD) of the two photometers as described in section 4. The fifth column shows the power spectrum for the difference (D) between the two photometers.

the two photometers and that the noise model is correct. They limit the magnitude of non-sky-stationary signals to a small fraction of the sky-stationary signal detected in the maps.

A series of Jack-knife tests shows agreement between the first and second halves of the flight (the difference of

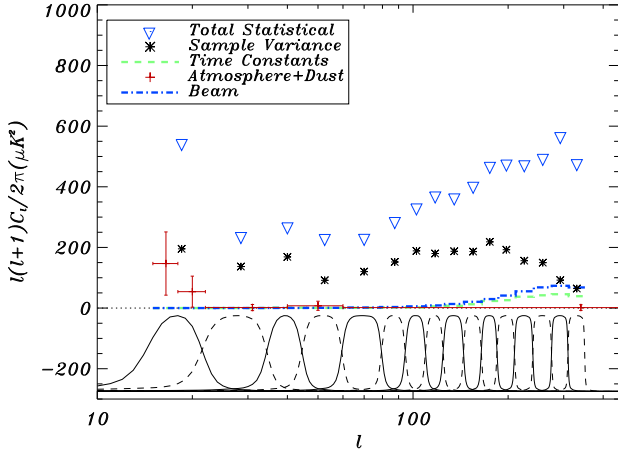


Fig. 3. Contamination by systematics : the Archeops CMB power spectrum statistical error bars (including noise and sample variance) are shown as the blue triangles. The large error bar in the first bin mainly comes from the high-pass filtering. The sample variance is shown as black stars. A conservative upper-limit to contamination by dust and atmospheric signal is shown in red crosses, with a ℓ different binning to enhance the low ℓ side. The effect of a 1σ beam and time constants uncertainty is shown as the dot-dashed blue and dashed green line respectively. The 7% temperature calibration uncertainty is not shown in the figure. At the bottom of the figure, the window functions for each multipole bin normalized to equal amplitude are represented.

the power spectra has $\chi^2/\text{nfd} = 21/16$), left and right halves of the map obtained with a cut in Galactic longitude ($\chi^2/\text{nfd} = 15/16$). Individual power spectra of the two photometers agree once absolute calibration uncertainties are taken into account. The power spectrum measured on the differences (D) between the two photometers is consistent with zero with a χ^2/nfd of 22/16 (Fig. 2) showing that the electromagnetic spectrum of the sky-stationary signal is consistent with that of the CMB. The measured CMB power spectrum depends neither on the Galactic cut (20, 30 and 40 degrees north from the Galactic plane), nor on the resolution of the maps (27, 14 and 7' pixel size, corresponding to $n_{\text{side}} = 128, 256$ and 512) nor on the TOI highpass filtering frequencies (0.3, 1 and 2 Hz).

Several systematic effects have been estimated and are summarized in Fig. 3, along with the statistical errors (blue triangles). The high frequency photometer (545 GHz) is only sensitive to dust and atmospheric emission, and thus offers a way to estimate the effect of any residual Galactic or atmospheric emission. Extrapolation of its power spectrum using a Rayleigh-Jeans spectrum times a ν^2 emissivity law between 545 and 217 GHz and as ν^0 between 217 and 143 GHz gives an upper-limit on the possible contamination by dust and atmosphere. The initial TOI was already decorrelated from the high frequency photometer and the residual contamination is estimated

to be much smaller than 50% of the initial one. The subsequent conservative upper-limit for dust and atmosphere contamination (50%) is shown in red crosses in Fig. 3. The contamination appears negligible in all bins but the first one ($\ell = 15$ to 22). High frequency spectral leaks in the filters at 143 and 217 GHz were measured to give a contribution less than half of the above contamination. In the region used to estimate the CMB power spectrum there are 651 extragalactic sources in the Parkes-MIT-NRAO catalog. These sources are mainly AGN, and their flux decreases with frequency. We have estimated their contribution to the power spectrum using the WOMBAT tools (Sokasian *et al.* 2001). At 143 (resp. 217) GHz this is less than 2 (resp. 1) percent of the measured power spectrum at $\ell \sim 350$. The beam and photometer time constant uncertainties were obtained through a simultaneous fit on Jupiter crossings. Their effect is shown as the dot-dashed blue and green-dashed lines in Fig. 3. The beam uncertainty includes the imperfect knowledge of the beam transfer function for each photometer's elliptical beam. Beam and time constants uncertainties act as a global multiplicative factor, but in the figure we show the 1σ effect on a theoretical power spectrum that has a good fit to the data. After the coaddition of the two photometers, the absolute calibration uncertainty (not represented in Fig. 3) is estimated as 7% (in CMB temperature units) with Monte-Carlo simulations.

As a final robustness test, the Archeops C_ℓ are computed using two additional independent methods. The first is based on noise estimation with an iterative multi-grid method, MAPCUMBA (Doré *et al.* 2001), simple map-making and C_ℓ estimation using SpICE (Szapudi *et al.* 2001) which corrects for mask effects and noise ponderation through a correlation function analysis. The second is based on MIRAGE iterative map-making (Yvon *et al.* 2002) followed by multi-component spectral matching (Cardoso *et al.* 2002, Patanchon *et al.* 2002). All methods use a different map-making and C_ℓ estimation method. Results between the three methods are in good agreement, which gives confidence in both the C_ℓ and in the upper-limits for possible systematic errors. Table 1 provides the angular power spectrum which is used for cosmological parameter extraction (Benoît *et al.* 2002b).

A comparison of the present results with other recent experiment and COBE/DMR is shown in Fig. 4. There is good agreement with other experiments, given calibration uncertainties, and particularly with the power COBE/DMR measures at low ℓ and the location of the first acoustic peak. Work is in progress to improve the intercalibration of the photometers, the accuracy and the ℓ range of the power spectrum: the low ℓ range will be improved increasing the effective sky area for CMB (which requires an efficient control of dust contamination), the high ℓ range will be improved by including more photometer pixels in the analysis.

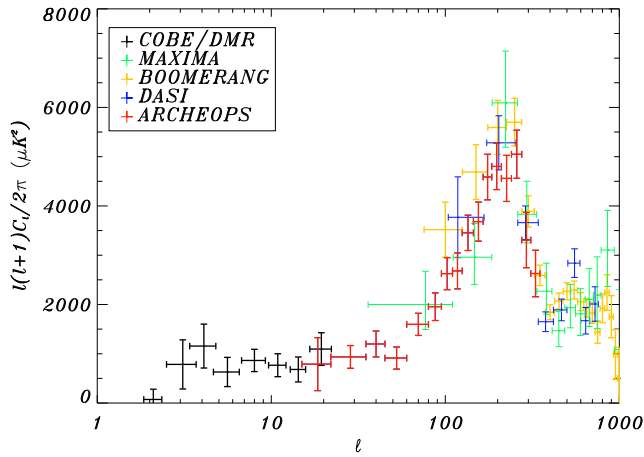


Fig. 4. The Archeops power spectrum compared with results of COBE, Boomerang, Dasi, Maxima (Tegmark *et al.* 1996, Netterfield *et al.* 2002, Lee *et al.* 2001, Halverson *et al.* 2002).

5. Conclusions

The Archeops experiment has observed a large portion of the sky. Maps from the two highest sensitivity detectors at 143 and 217 GHz show consistent, sky-stationary anisotropy signal that appears inconsistent with any known astrophysical source other than CMB anisotropy. The angular power spectrum of this signal at multipoles between $\ell = 15$ and $\ell = 350$ shows a clear peak at $\ell \simeq 200$. These results are consistent with predictions by inflationary-motivated cosmologies. Archeops provides the highest signal-to-noise ratio mapping of the first acoustic peak and its low- ℓ side of any experiment to date and covers the largest number of decades in ℓ . It has been obtained with a limited integration time (half a day) using a technology similar to that of the Planck HFI experiment. An extensive set of tests limits the contribution of systematic errors to a small fraction of the statistical and overall calibration errors in the experiment. More data reduction is under way to increase the accuracy and ℓ range of the power spectrum. The determination of cosmological parameters are discussed in a companion paper (Benoît *et al.* 2002b).

Acknowledgements. The authors would like to thank the following institutes for funding and balloon launching capabilities: CNES (French space agency), PNC (French Cosmology Program), ASI (Italian Space Agency), PPARC, NASA, the University of Minnesota, the American Astronomical Society and a CMBNet Research Fellowship from the European Commission. Healpix package was used throughout the data analysis (Gorski *et al.* 1998).

References

Benoît, A. *et al.* 2002a, *Astropart.Phys.*, 17, 101
 Benoît, A. *et al.* 2002b, *A&A*, submitted
 Benoît, A. *et al.* 2002c, in preparation

Benoît, A. *et al.* 2002d, in preparation
 Benoît, A. *et al.* 2002e, in preparation
 de Bernardis, P. *et al.* 2000, *Nature*, 404, 955
 Cardoso, J. F., Snoussi, H., Delabrouille, J., Patanchon, G. 2002, *astro-ph/0209466*
 Doré, O. *et al.* 2001, *A&A*, 374, 358
 Ferreira, P. G. *et al.* 1999, *ApJ*, 515, L1
 Fosalba, P. *et al.* 2002, *Phys.Rev.D*, 65, 63003
 Gorski, K. M. *et al.* 1998, *astro-ph/9812350*, <http://www.eso.org/science/healpix>
 Halverson, N. W. *et al.* 2002, *ApJ*, 568, 38
 Hanany, S. *et al.* 2000, *ApJ*, 545, L5
 Hivon, E. *et al.* 2001, *astro-ph/0105302*
 Lee, A. T. *et al.* 2001, *ApJ*, 561, L1
 Miller, A. D. *et al.* 1999, *ApJ*, 524, L1
 Netterfield, C. B. *et al.* 2002, *ApJ*, 571, 604
 Patanchon, G., Delabrouille, J. *et al.* 2002, in preparation.
 Rubiño-Martin J. A. *et al.* 2002, *astro-ph/0205367*
 Schlegel, D. J., Finkbeiner, D. P., Davis, M. 1998, *ApJ*, 500, 525
 Sievers, J. L. *et al.* 2002, *astro-ph/0205387*.
 Smoot, G. F. *et al.* 1992, *ApJ*, 395, L1
 Sokasian, A., Gawiser, E., Smoot, G. F. 2001, *ApJ*, 562, L88
 Stompor, R. *et al.* 2001, *ApJ*, 561, L7
 Szapudi, I. *et al.* 2001, *ApJ*, 548, L115
 Tegmark, M. *et al.* 1996, *ApJ*, 464, L35
 Yvon, D. *et al.* 2002, in preparation.